



Application of $\text{TiO}_2/\text{ZnFe}_2\text{O}_4$ /glycine nanocatalyst to the treatment of methyl orange dye from aqueous solution: Impacts of dissolved mineral salts on dye removal efficiency

M. Hajiali, M. Farhadian*, S. Aflaki, and N. Davari

Department of Chemical Engineering, Faculty of Engineering, University of Isfahan, Isfahan, Iran.

Received 15 July 2020; received in revised form 7 November 2020; accepted 15 March 2021

KEYWORDS

Methyl orange;
 Photocatalysis;
 $\text{TiO}_2/\text{ZnFe}_2\text{O}_4$ /glycine;
 Mineral salts;
 Reaction rate constant.

Abstract. This study aims to remove one of the frequently used dyes in textile industries, i.e., Methyl Orange, from polluted water with $\text{TiO}_2/\text{ZnFe}_2\text{O}_4$ /glycine catalyst under UV irradiation. The TiO_2 /glycine/ ZnFe_2O_4 nanocatalyst was synthesized using the sol-gel method and characterized by XRD, XRF, FT-IR, UV-visible DRS, BET, FE-SEM, and EDX analyses. Process factors including initial dye concentration (10–30 ppm), catalyst dosage (0.5–1.5 g/L), initial pH solution (3–11), and irradiation time (30–150 min) were investigated by central composite design. The removal efficiency of methyl orange was 80% under the optimal conditions, i.e., dye concentration of 20 ppm, catalyst dosage of 1 g/L, irradiation time of 120 min, and pH = 6.5. The effects of mineral salts such as NaHCO_3 , NaCl , Na_2SO_4 , KCl , MgSO_4 , and CaCl_2 with the concentrations of 50–800 ppm on the dye removal efficiency were evaluated under optimal conditions. Although low concentrations of NaCl , KCl , and CaCl_2 had adverse effects on MO removal efficiency, the dye removal efficiency was enhanced at their high levels ($R_{\text{NaCl},800} = 74.52\%$). An increase in the concentrations of MgSO_4 and Na_2SO_4 produced deactivation effects on the dye removal efficiency and reaction rate constant (MgSO_4 deactivation: 36%). The pollutant removal efficiency and reaction rate constant increased using NaHCO_3 ($R_{\text{NaHCO}_3,800} = 82.4\%$ and $k_{\text{NaHCO}_3,800} = 20.84 \text{ day}^{-1}$).

© 2021 Sharif University of Technology. All rights reserved.

1. Introduction

Methyl Orange (MO), which belongs to azo dyes, is widely used in textile, food, paper, leather, printing, and pharmaceutical industries [1,2]. Wastewater containing MO has devastating effects on the environment due to its toxicity, carcinogenicity, mutagenicity, non-biodegradability, and complex chemical structure [3–

6]. In recent years, researchers have studied the role of Advanced Oxidation Processes (AOPs) in removing dyes from wastewater. Based on the generation of hydroxyl radicals for degrading pollutants, these techniques are characterized by high removal efficiency with no secondary contamination being produced [7,8]. Among AOPs, photocatalysis is a promising technology for the treatment of dyes from pollutant water due to its high efficiency in removing non-biodegradable contaminants [9–12]. A green photocatalyst, TiO_2 , has received considerable attention in the case of photocatalysis owing to its high photoactivity, outstanding stability, and non-toxic nature [13,14]. However, the

*. Corresponding author. Tel.: 0098 313 7937032
 E-mail address: m.farhadian@eng.ui.ac.ir (M. Farhadian)

applicability of pure TiO₂ in the visible light region is limited since it experiences a wide bandgap (3.2 eV) and a rapid recombination rate of electron-hole pairs [15]. In order to modify the TiO₂ bandgap and reduce the recombination rate of electron-hole pairs, doping this photocatalyst with semiconductors and non-metal elements is of significance in enhancing TiO₂ performance [16]. For this reason, ZnFe₂O₄ semiconductor has been used owing to its narrow bandgap energy (1.9 eV), strong photochemical stability, and low cost [17]. Another dopant is glycine that consists of carbon and nitrogen elements, and it is also non-toxic and inexpensive [18].

To the best of our knowledge, no study has reported the removal of MO from polluted water using TiO₂/ZnFe₂O₄/glycine catalyst in the presence of mineral salts. The objective of this study was to investigate the treatment of MO from aqueous solution with TiO₂/ZnFe₂O₄/glycine under UV irradiation. The catalyst is synthesized using the sol-gel method and is characterized by XRD, XRF, FT-IR, UV-visible DRS, BET, FE-SEM, and EDX analyses. Process factors including initial dye concentration, catalyst dosage, initial pH solution, and irradiation time were investigated using Response Surface Methodology (RSM). Moreover, the effects of the concentrations of mineral salts such as NaHCO₃, NaCl, Na₂SO₄, KCl, MgSO₄, and CaCl₂ on the dye removal efficiency were examined under optimal conditions.

2. Material and methods

2.1. Materials

The chemicals used for preparation of TiO₂/ZnFe₂O₄/Glycine nanocatalyst were FeN₃O₉.9H₂O (CAS# 10421484, purity 98%), Zn(NO₃)₂.6H₂O (CAS# 7779886, purity 99%), citric acid (CAS# 77929, purity 99%), glycine (CAS# 56406, purity 99%), tetrabutyl orthotitanate (CAS# 5593704, purity 99%), ethanol (CAS# 64174, purity 99%), and HCl (CAS# 7647010,

purity 30%). Moreover, NaOH (CAS#1310732, purity 95%) and H₂SO₄ (CAS#7664939, purity 97%) were used to adjust the pH of the solution. All of the used chemicals along with MO dye and some mineral salts such as NaCl, NaHCO₃, KCl, Na₂SO₄, CaCl₂, and MgSO₄ were purchased from Merck Company, Germany. The properties of MO dye are presented in Table 1.

2.2. Synthesis of TiO₂/ZnFe₂O₄/glycine catalyst

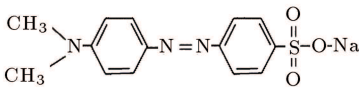
Based on the screening experiments, the optimal weight ratios of TiO₂/glycine-5% and TiO₂/glycine/ZnFe₂O₄-35% were taken into account in this study. First, to synthesize ZnFe₂O₄ catalyst (1 g), FeN₃O₉.9H₂O solution (1 M, 8.3 mL) and Zn(NO₃)₂.6H₂O solutions (1 M, 4.15 mL) were mixed. Next, citric acid solution (1 M, 18.7 mL) was added to the above solution. The final solution was stirred at 100°C for 1 h to form a gel. The process ended with drying of the obtained gel in an oven at 120°C for 24 h and calcination of ZnFe₂O₄ catalyst in a muffle furnace at 500°C for 2 h [19]. To synthesize TiO₂/ZnFe₂O₄/glycine (1 g) using the sol-gel method, tetrabutyl orthotitanate (16 mL) was first added dropwise into ethanol (20 mL) with a molar ratio of TiO₂/C₂H₅OH (1:15). In addition, ZnFe₂O₄ (2 g) and glycine (0.2 g) were dissolved in ethanol and deionized water, respectively. Then, the solution underwent ultrasound at 80°C for 30 min, and HCl, glycine, and ZnFe₂O₄ solutions were added dropwise into tetrabutyl orthotitanate solution, respectively. The obtained solution was stirred at 80°C to form a gel.

Finally, the gel was dried in an oven at 120°C for 24 h, and the calcination process was performed in a muffle furnace at 450°C for 2 h to achieve TiO₂/ZnFe₂O₄/glycine nanocatalyst [20].

2.3. Characterization

Some analyses were conducted to characterize TiO₂/ZnFe₂O₄/glycine catalyst. For instance, XRD

Table 1. Characteristics of MO dye.

Dye name	Methyl Orange (MO)
Type	Azo dye
Chemical formula	C ₁₄ H ₁₄ N ₃ NaO ₃ S
Chemical structure	
Molecular weight (g/mol)	327.33
Solubility (mg/L)	5000
λ _{max} (nm)	465
pK _a	3.4

analysis was employed to detect TiO_2 and ZnFe_2O_4 by an X-ray diffraction device (D-8 Advance, Bruker, Germany). Based on the XRD analysis and Scherrer equation, the crystallite size of the nanocatalyst was determined by Eq. (1).

$$D = \frac{K\lambda}{B \cos \theta}, \quad (1)$$

where D is the crystallite size (average in Å), K the shape factor (0.9), λ the wavelength of the used X-ray (1.54 Å), B the width of the maximum peak at half of its height (FWHM), and θ half of the Bragg angle (in terms of radiant).

XRF analysis was performed to determine the composition of the compounds in the synthesized nanocatalyst by an X-ray fluorescence device (S4-Pioneer, Bruker, Germany). To determine the functional groups of the nanocatalysts, FT-IR analysis was performed using a Fourier transform infrared spectrometer device (FT-IR-6899, Jasco, Japan). Further, BET analysis was conducted to investigate the surface area, pore-volume, and average pore diameter of the nanocatalyst by measuring N_2 adsorption at 77 K (Bell 12, Japan). Electron microscopy images were taken by an FE-SEM device (S-4160, Hitachi, Japan), and the morphology and structure of the nanocatalyst were examined by a scanning electron microscopy device (SEM, XL series, Phillips XL30) equipped with EDX analysis (MIRA3, Tescan, Czechia). Furthermore, UV-Vis DRS analysis was carried out to measure the bandgap energy of the nanocatalyst using an ultraviolet-visible spectrophotometer device (V-670, Jasco, Japan). The bandgap energy of $\text{TiO}_2/\text{ZnFe}_2\text{O}_4/\text{glycine}$ nanocatalyst was calculated by Tauc plot through the following equations:

$$\alpha(h\nu) = (h\nu - E_g)^{1/n}, \quad (2)$$

$$h\nu = \frac{1240}{\lambda}, \quad (3)$$

where E_g is the bandgap energy (eV), α the absorption coefficient, h the Planck's constant, and ν the light frequency. n equals 0.5 or 2 depending on the nature of the electron transition, and λ is the wavelength of the absorption edge in the spectrum (nm).

2.4. Photocatalytic removal experiments

Photocatalytic experiments for MO removal were carried out in a cylindrical reactor (200 mL) with a UV lamp (11 W and 254 nm). The reactor was covered by a water circulation system and equipped with a thermometer to adjust the reactor temperature at $25 \pm 2^\circ\text{C}$. Figure 1 shows the experimental setup.

According to Table 2, an MO solution was prepared for each photocatalytic experiment, and H_2SO_4 and NaOH adjusted the pH of the MO solution via a pH meter (UB-10, Denver). The MO solution and a specific concentration of $\text{TiO}_2/\text{ZnFe}_2\text{O}_4/\text{glycine}$ nanocatalyst were transferred to the reactor. Followed by conducting the MO photocatalytic experiments at the determined irradiation time, a nanocatalyst was separated from the MO solution by a centrifuge device (Supra 22K, Hanil) at 10000 rpm for 20 min. The final MO concentration was measured using a UV-VIS spectrophotometer (V-570, Jasco, Japan) at $\lambda_{\text{max}} = 465$ nm. The efficiency of MO (R) removal was calculated by Eq. (4):

$$R = \frac{C_i - C_f}{C_i} \times 100\%, \quad (4)$$

where C_i and C_f are the initial and final concentrations of MO (mg/L), respectively.

Furthermore, to investigate the effects of mineral

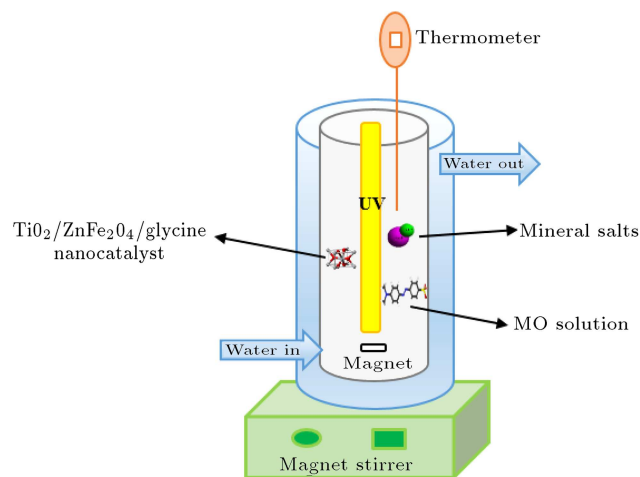


Figure 1. Experimental setup.

Table 2. Selected factors and levels for MO removal.

Factors	Symbol	Levels				
		-2	-1	0	+1	+2
pH	A	3	5	7	9	11
Dye concentration (ppm)	B	10	15	20	25	30
Catalyst dosage (g/L)	C	0.5	0.75	1	1.25	1.5
Irradiation time (min)	D	30	60	90	120	150

salts on MO removal efficiency under optimal conditions, NaHCO₃, NaCl, Na₂SO₄, KCl, MgSO₄, and CaCl₂ with concentrations of 50, 100, 200, 400, and 800 ppm, respectively, were taken into account. Reaction rate constant (k) was calculated by the following equation at 30 min time intervals:

$$-r_A = \frac{dC_A}{dt} = kC_A^n \quad (5)$$

In Eq. (5), $-r_A$, k , C_A , and t are the reaction rate, reaction rate constant, MO concentration, and reaction time, respectively.

2.5. Experimental design

One of the commonly used models of RSM, i.e., Central Composite Design (CCD), was used to examine the effects of process factors on MO removal efficiency using TiO₂/ZnFe₂O₄/glycine catalyst. Based on the primary screening experiments, the process factors including pH, dye concentration, catalyst dosage, and irradiation time were selected, and other parameters such as temperature (25 ± 2°C) and UV lamp radiation (11 W, 254 nm) were kept constant. Table 2 presents the selected factors and levels required for MO removal.

Based on Eq. (6), for four factors, five levels, and six central point replications, 30 experiments were designed through the Design-Expert 10.0.7 software:

$$N = 2^k + 2k + n_0, \quad (6)$$

where N , k , and n_0 are the numbers of total runs, factors, and central point replications, respectively.

3. Results and discussion

3.1. Characterization of

TiO₂/ZnFe₂O₄/glycine catalyst

The XRD pattern of TiO₂/ZnFe₂O₄/glycine catalyst is illustrated in Figure 2. The main peaks at 2θ values of 25.41°, 38.05°, 48.03°, and 54.94° belonged to Anatase

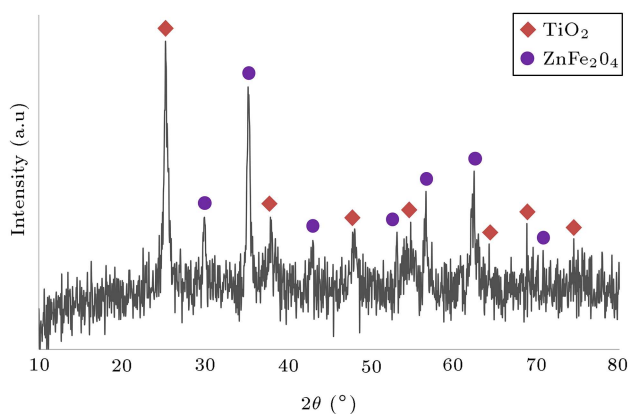


Figure 2. XRD pattern of TiO₂/ZnFe₂O₄/glycine catalyst.

Table 3. XRF analysis of TiO₂/ZnFe₂O₄/glycine catalyst.

Compound	Concentration (W/W%)
TiO ₂	63.47
Fe ₂ O ₃	24.26
ZnO	11.033
Al ₂ O ₃	0.067
Cl	1.08
CuO	0.042
SiO ₂	0.048
Total	100

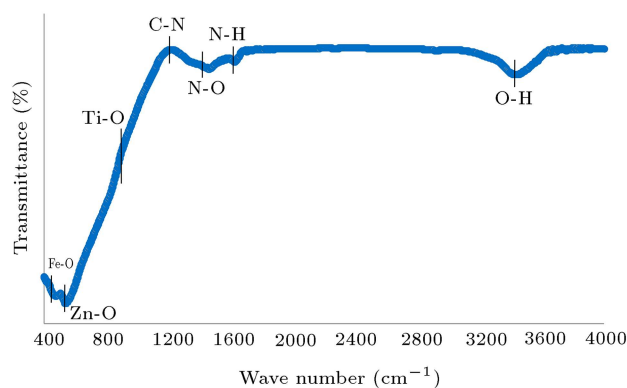


Figure 3. FT-IR spectrum of TiO₂/ZnFe₂O₄/glycine catalyst.

TiO₂ phase [21]. In addition, ZnFe₂O₄ at 2θ values of 29.89°, 35.24°, and 62.28° had major peaks, which confirmed the Franklinitite phase [22]. However, Figure 2 does not depict the peaks of nitrogen and carbon due to their low glycine concentration. According to Eq. (1), the crystallite size of TiO₂/ZnFe₂O₄/glycine catalyst was calculated as 8.14 nm.

According to the results of XRF shown in Table 3, TiO₂/ZnFe₂O₄/glycine nanocatalyst consists of 63.47 Wt% of TiO₂ and 11.03 Wt% of ZnO. The precalculated value of the weight ratio of ZnFe₂O₄/(TiO₂/glycine) in the catalyst (0.5) was also successfully obtained.

FT-IR spectrum of the TiO₂/ZnFe₂O₄/glycine catalyst (Figure 3) shows the peaks of Fe-O, Zn-O, and Ti-O functional groups at the wavenumbers of approximately 462, 544, and 873 cm⁻¹, respectively [23,24]. Furthermore, C-N, N-O, N-H, and O-H functional groups had wavenumbers of about 1339, 1462, 1610, and 3428 cm⁻¹, respectively, confirming the presence of Glycine in the catalyst [25].

The UV-Vis DRS spectrum of TiO₂/ZnFe₂O₄/glycine nanocatalyst (Figure 4(a)) indicates the high absorption intensity of the nanocatalyst in the vis-

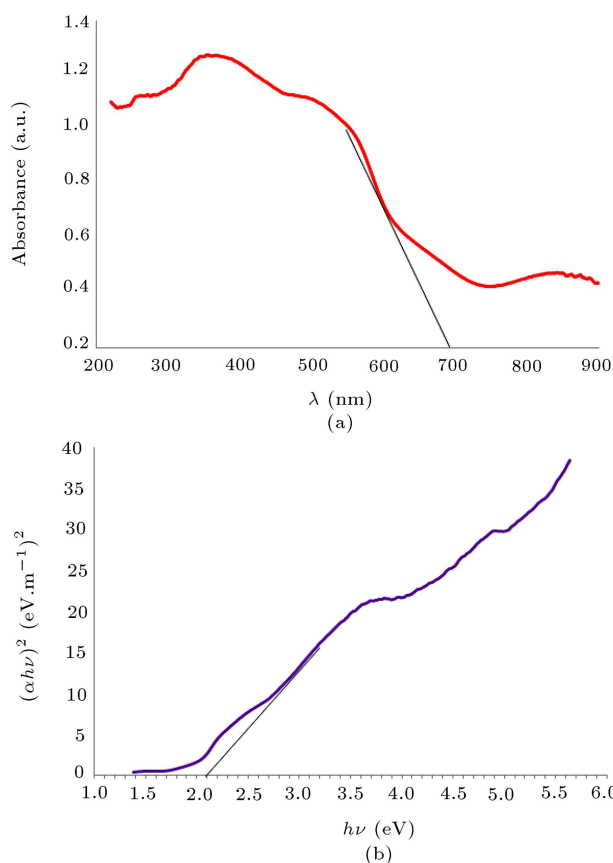


Figure 4. (a) UV-Vis DRS spectrum of $\text{TiO}_2/\text{ZnFe}_2\text{O}_4/\text{glycine}$ catalyst. (b) Bandgap energy determination of $\text{TiO}_2/\text{ZnFe}_2\text{O}_4/\text{glycine}$ catalyst.

ible light region (absorption edge of 700 nm). As observed in Figure 4(b), the bandgap energy of $\text{TiO}_2/\text{ZnFe}_2\text{O}_4/\text{glycine}$ nanocatalyst was calculated as 2.1 eV using the Tauc plot (Eqs. (2) and (3)). The obtained results given in Figure 4 can be verified by the photogenerated electron transition in the ZnFe_2O_4 energy band structure, which increased the mobility and absorption of the carrier and decreased the bandgap energy in the catalyst [22] compared to TiO_2 with an absorption edge of 390 nm and bandgap energy of 3.2 eV.

BET analysis of $\text{TiO}_2/\text{ZnFe}_2\text{O}_4/\text{glycine}$ is presented in Table 4. According to the results, the catalyst covers a BET surface area of $56.239 \text{ m}^2/\text{g}$, an average pore diameter of 7.559 nm, and a total pore volume of $0.106 \text{ cm}^3/\text{g}$.

The EDX spectrum of $\text{TiO}_2/\text{ZnFe}_2\text{O}_4/\text{glycine}$ catalyst (Figure 5) confirms the presence of several elements such as Ti (40.25%), O (34.83%), Fe (10.12%), C (6.41%), Zn (5.62%), and N (2.77%).

Moreover, the FE-SEM image of $\text{TiO}_2/\text{ZnFe}_2\text{O}_4/\text{glycine}$ catalyst (Figure 6(a)) is indicative of the porous structures with particle sizes of 24.31, 33.54, and 26.73 nm, respectively. Particle size distribution of $\text{TiO}_2/\text{ZnFe}_2\text{O}_4/\text{glycine}$ catalyst was measured using

Table 4. BET analysis of $\text{TiO}_2/\text{ZnFe}_2\text{O}_4/\text{glycine}$ catalyst.

Parameter (unit)	Value
BET surface area (m^2/g)	56.239
Langmuir surface area (m^2/g)	60.269
External surface area (m^2/g)	35.494
Microporesurface area (m^2/g)	43.652
Total pore volume (cm^3/g)	0.106
Average pore diameter (nm)	7.559

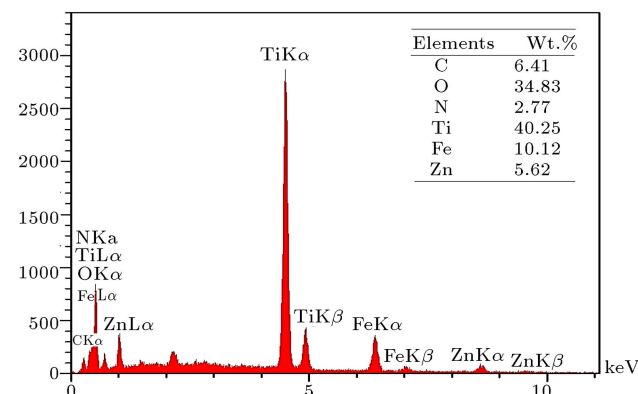


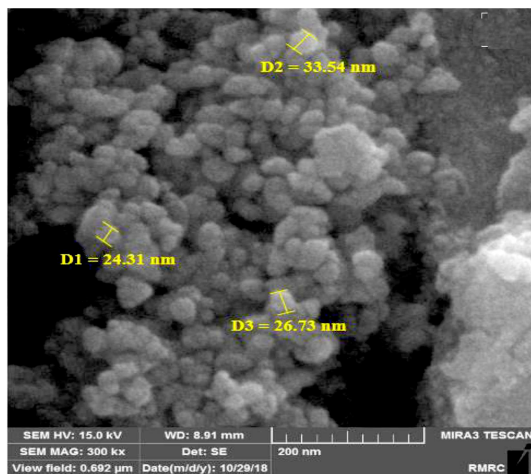
Figure 5. EDX spectrum of $\text{TiO}_2/\text{ZnFe}_2\text{O}_4/\text{glycine}$ catalyst.

Image J 1.44p software. According to Figure 6(b), the particle size distribution of the catalyst was between 1 and 80 nm, and most of particle sizes were below 10 nm.

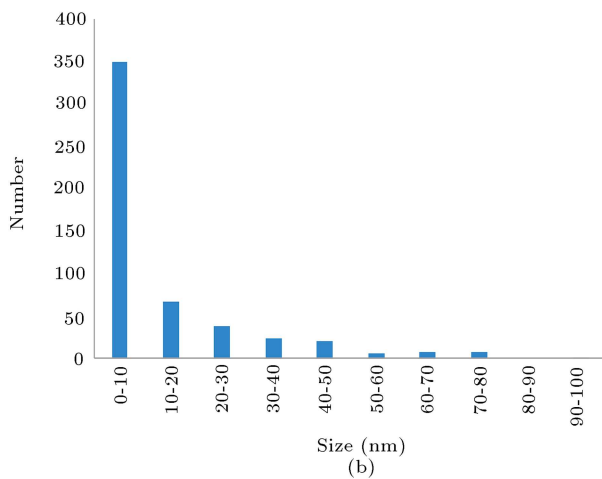
The point of zero charge (pH_{pzc}) for $\text{TiO}_2/\text{ZnFe}_2\text{O}_4/\text{glycine}$ catalyst was determined based on the pH drift method by intersecting the pH curve with the $y = x$ line [26]. Based on Figure 7, the pH_{pzc} of $\text{TiO}_2/\text{ZnFe}_2\text{O}_4/\text{glycine}$ catalyst was measured as 7.2.

3.2. Results of photocatalytic experiments on MO removal efficiency

The results of Analysis of Variance (ANOVA) for MO removal efficiency are reported in Table 5. In this regard, the P -value and F -value were considered as two indices indicating the significance of factors and priority of influence of factors, respectively. The factor with a P -value of < 0.05 was a significant factor (confidence interval: 95%). The model presented in Table 5 was also significant ($P < 0.0001$). Moreover, the pH, MO concentration, irradiation time, interaction between the pH and catalyst dosage, and interaction between the irradiation time and MO concentration were significant factors. According to F -value, the MO concentration, irradiation time, pH, and catalyst dosage had maximum effects on MO removal efficiency ranked in order.



(a)



(b)

Figure 6. (a) FE-SEM image of $\text{TiO}_2/\text{ZnFe}_2\text{O}_4/\text{glycine}$ catalyst. (b) Particle size distribution of $\text{TiO}_2/\text{ZnFe}_2\text{O}_4/\text{glycine}$ catalyst.

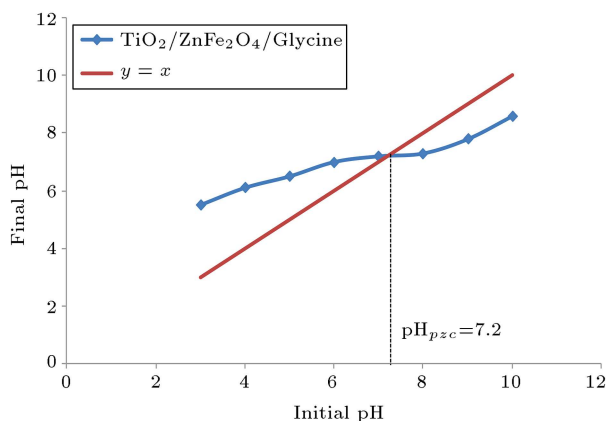
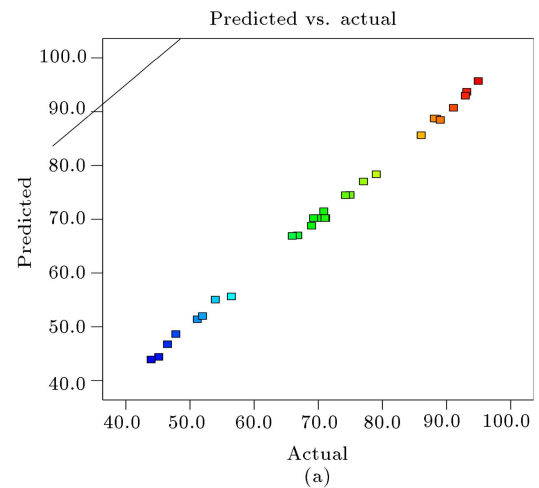
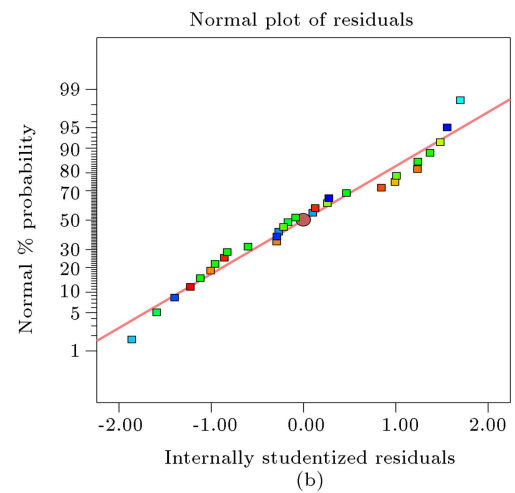


Figure 7. pH_{pzc} for $\text{TiO}_2/\text{ZnFe}_2\text{O}_4/\text{glycine}$ catalyst.

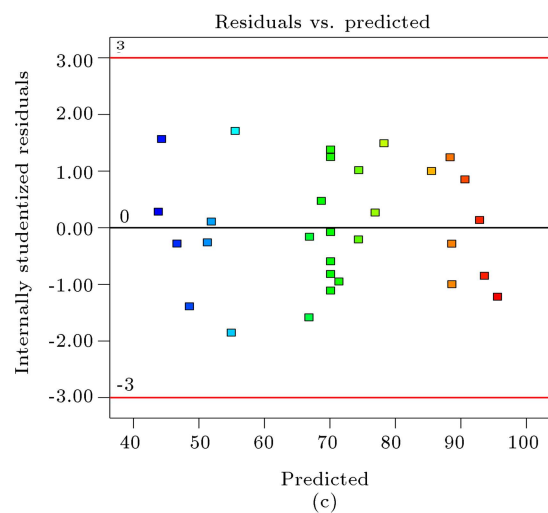
Figure 8(a) indicates that the experimental results were well fitted with the data of the predicted model in terms of MO removal efficiency. The values of R^2 (0.9985) and adjusted R^2 (0.9972) proved the



(a)



(b)



(c)

Figure 8. Plots of (a) predicted values vs. actual results, (b) normal probability vs. residuals, and (c) internally studentized residuals vs. predicted results for MO removal.

accuracy and acceptability of the model used in this study. Figure 8(b) confirms the efficiency of the proposed model by plotting the normal probability of the residuals. Furthermore, Figure 8(c) presents a com-

Table 5. ANOVA for MO removal.

Source	Sum of squares	df	Mean square	F-value	p-value	Status
Model	7064.01	14	504.57	737.27	< 0.0001	Significant
A (pH)	5.95	1	5.95	8.69	0.0100	Significant
B (MO concentration)	3202.82	1	3202.82	4679.90	< 0.0001	Significant
C (catalyst dosage)	0.5370	1	0.5370	0.7847	0.3897	Not significant
D (irradiation time)	2377.85	1	2377.85	3474.47	< 0.0001	Significant
AB	6.57	1	6.57	9.59	0.0074	Significant
AC	227.63	1	227.63	332.61	< 0.0001	Significant
AD	0.2783	1	0.2783	0.4066	0.5333	Not significant
BC	0.3752	1	0.3752	0.5482	0.4705	Not significant
BD	33.32	1	33.32	48.69	< 0.0001	Significant
CD	0.0150	1	0.0150	0.0219	0.8843	Not significant
A ²	653.17	1	653.17	954.40	< 0.0001	Significant
B ²	0.2166	1	0.2166	0.3164	0.5821	Not significant
C ²	379.08	1	379.08	553.90	< 0.0001	Significant
D ²	4.73	1	4.73	6.91	0.0190	Significant
Lack of fit	7.00	10	0.7004	1.07	0.4996	Not significant

parison between the internally studentized residuals and predicted results, indicating the high efficiency of the presented model or the assumption of the constant variance.

The quadratic model for MO removal efficiency is shown in Eq. (7).

$$\begin{aligned}
 R(\%) = & + 70.16 - (0.49 \times A) - (11.55 \times B) \\
 & + (0.15 \times C) + (9.95 \times D) + (0.64 \times AB) \\
 & + (3.77 \times AC) - (0.13 \times AD) - (0.15 \times BC) \\
 & + (1.44 \times BD) - (0.03 \times CD) + (4.88 \times A^2) \\
 & - (0.09 \times B^2) - (3.72 \times C^2) - (0.41 \times D^2). \quad (7)
 \end{aligned}$$

The percentage effect of each factor on MO removal efficiency was determined by Pareto analysis (Eq. (8)):

$$P_i = \left(\frac{b_i^2}{\sum b_i^2} \right) \times 100\%, \quad (8)$$

where b_i is the coefficient of each factor, and P_i is the percentage effect.

The results revealed that MO concentration (B : 46.44%) had the most significant effect on MO removal efficiency.

3.3. Effects of process factors on MO removal efficiency

The effects of MO concentration and irradiation time on MO removal efficiency are presented in Figure 9(a)

(catalyst dosage = 1 g/L and pH = 7). Although MO removal showed maximum efficiency at low dye concentrations, it decreased at high concentrations of MO. When MO concentration increased from 10 to 20 ppm at the irradiation time duration of 90 min, MO removal efficiency decreased from 92.9 to 70.2%. With further increase in MO concentration to 30 ppm at the same irradiation time, MO removal efficiency decreased to 46.7%, mainly because the catalyst surface was saturated at high MO concentrations, thus attenuating the activation of the catalyst in generating electron-hole pairs and hydroxyl radicals [27,28]. As shown in Figure 9(a), the removal of MO with TiO₂/ZnFe₂O₄/glycine nanocatalyst occurred within a longer irradiation time span due to the complex structure of the dye [29]. In an MO concentration of 20 ppm, MO removal efficiency increased from 48.6 to 70.2%, with the irradiation time increasing from 30 to 90 min. Then, MO removal efficiency reached 88.4% after 150 min. Moreover, in MO concentrations of 10–13 ppm, MO was completely removed within approximately 120 min. However, at MO concentrations greater than about 13 ppm, the removal efficiency reached 100% after 150 min mainly due to the interaction between irradiation time and MO concentration. Figure 9(b) shows the effects of catalyst dosage and MO concentration on MO removal efficiency (pH = 7 and irradiation time = 90 min). Upon an increase in TiO₂/ZnFe₂O₄/glycine catalyst dosage from 0.5 to 1 g/L in an MO concentration of 20 ppm, MO removal efficiency first increased by 15.2%

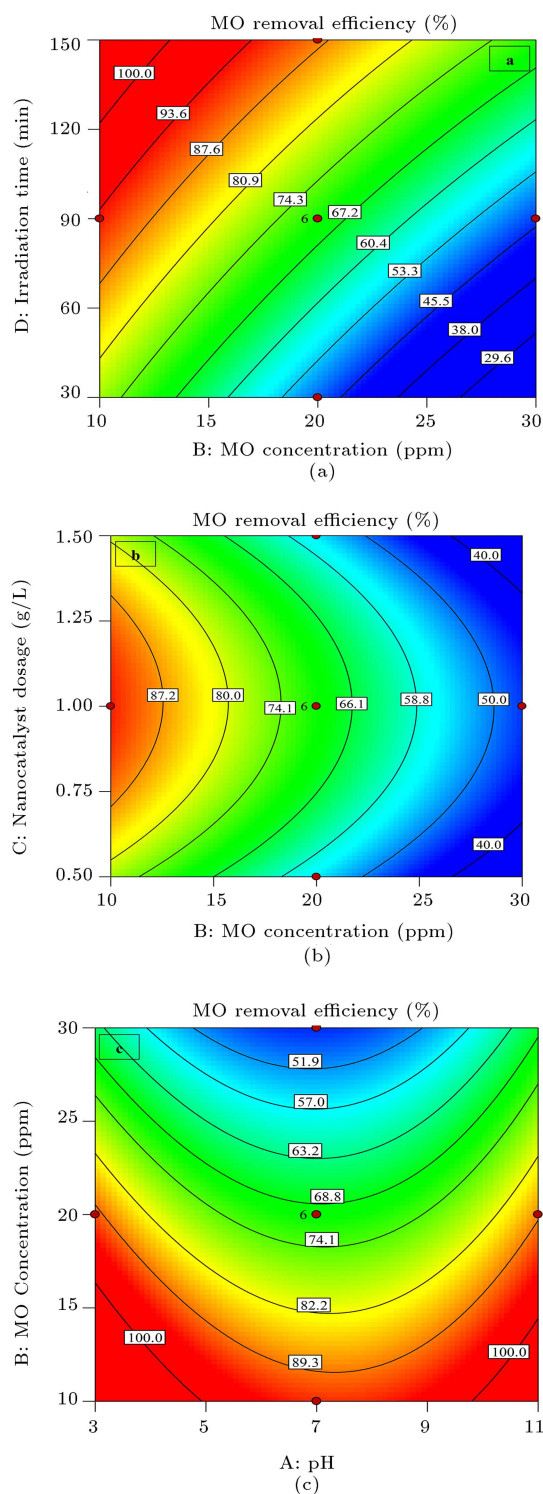


Figure 9. Counter plots of MO removal efficiency as (a) irradiation time and MO concentration, (b) catalyst dosage and MO concentration, and (c) MO concentration and pH.

and then, decreased by 14.6% at a catalyst dosage of 1.5 g/L. These results can be confirmed based on the report of the active sites for the catalyst. At low catalyst dosages, MO removal efficiency would rise

owing to the detected active sites on the surface of the catalyst and the increased UV permeation through the catalyst. However, high catalyst dosages would lessen MO removal efficiency since the catalysts blocked the UV permeation and developed the turbidity [7,30]. The effects of pH and MO concentration on MO removal efficiency are illustrated in Figure 9(c) (catalyst dosage = 1 g/L and irradiation time = 90 min). There was a 20.5% decline in MO removal efficiency with an increase in pH from 3 to 7 in the dye concentration of 20 ppm. In addition, a rise in pH from 7 to 9 led to an increase in MO removal efficiency from 70.2 to 74.5%, and the removal efficiency increased to 88.7% at pH = 11. Under acidic conditions, $\text{TiO}_2/\text{ZnFe}_2\text{O}_4/\text{glycine}$ catalyst is positively charged for $\text{pH} < \text{pH}_{\text{pzc}}$. Therefore, MO removal efficiency increased due to electrostatic attraction [31]. After that, MO removal efficiency declined following an increase in pH to 7. At an alkaline pH, hydroxyl radicals are produced more rapidly thanks to their high concentrations [32], resulting in reacting more readily with MO and increasing MO removal efficiency.

The predicted removal efficiency of MO was 80.2% under optimal conditions (dye concentration = 20 ppm, catalyst dosage = 1 g/L, irradiation time = 120 min, and pH = 6.5). To verify the prediction results of the presented model, experiments were carried out under optimal conditions and the removal efficiency was measured at 80%.

3.4. Effects of mineral salts on MO removal efficiency

To investigate the effects of mineral salt concentrations on MO removal efficiency, the removal efficiency was considered at 80% under the following optimal process conditions: MO concentration of 20 ppm, $\text{TiO}_2/\text{ZnFe}_2\text{O}_4/\text{glycine}$ catalyst dosage of 1 g/L, irradiation time of 120 min, and pH = 6.5. The impacts of mineral salts, including NaHCO_3 , NaCl , Na_2SO_4 , KCl , MgSO_4 , and CaCl_2 on MO removal efficiency under optimal conditions are reported in Table 6.

3.4.1. Chloride ions

Low concentrations of NaCl , KCl , and CaCl_2 had adverse effects on the dye removal efficiency and reaction rate constant due to the formation of fouling on the catalyst [33], such that NaCl at a concentration of 50 ppm experienced the minimum removal efficiency of 66.96% and reaction rate constant of 13.27 day^{-1} . However, ionic strengths of NaCl , KCl , and CaCl_2 at high concentrations increased MO removal efficiency and reaction rate constant ($k_{\text{NaCl},800} = 16.36 \text{ day}^{-1}$ and $R_{\text{NaCl},800} = 74.52\%$). This increase occurred because high ionic strength reduced the dye resistance to the surface of the catalyst by compressing the electric layer, resulting in greater adsorption [33].

Table 6. Effects of mineral salts on MO removal efficiency and reaction rate constant (TiO₂/ZnFe₂O₄/glycine catalyst dosage: 1 g/L, MO concentration: 20 ppm, pH: 6.5, and irradiation time: 120 min).

Mineral salts	Concentration (ppm)	k (day ⁻¹)	R (%)	pH	r^2	Mineral salts	Concentration (ppm)	k (day ⁻¹)	R (%)	pH	r^2
NaHCO ₃	50	14.89	71.27	7.5	0.9881	NaCl	50	13.27	66.96	6.5	0.9989
	100	16.33	74.45	8.3	0.9825		100	15.07	71.58	6.5	0.9950
	200	17.65	77.10	8.7	0.9862		200	15.98	73.78	6.5	0.9831
	400	17.89	77.49	9.1	0.9822		400	16.06	73.83	6.5	0.9910
	800	20.84	82.40	9.1	0.9972		800	16.36	74.52	6.5	0.9958
Na ₂ SO ₄	50	15.23	72.23	6.5	0.9971	KCl	50	13.83	68.37	6.5	0.9894
	100	15.15	71.70	6.5	0.9948		100	15.02	71.43	6.5	0.9923
	200	14.64	70.52	6.5	0.9916		200	15.74	73.08	6.5	0.9955
	400	13.23	66.81	6.5	0.9956		400	15.75	73.09	6.5	0.9953
	800	13.01	66.20	6.5	0.9800		800	15.93	73.48	6.5	0.9966
MgSO ₄	50	13.42	67.34	6.5	0.9857	CaCl ₂	50	14.73	70.75	6.5	0.9989
	100	13.21	66.76	6.5	0.9861		100	14.93	71.17	6.5	0.9954
	200	12.91	65.47	6.5	0.9883		200	15.28	72.10	6.5	0.9969
	400	12.65	65.29	6.5	0.9889		400	15.42	72.35	6.5	0.9996
	800	12.34	64.26	6.5	0.9874		800	15.47	72.49	6.5	0.9997

The influences of NaCl, KCl, and CaCl₂ on the dye removal efficiency and reaction rate constant were Ca²⁺ > K⁺ > Na⁺ at low concentrations and Ca²⁺ < K⁺ < Na⁺ at high levels [21,34].

3.4.2. Bicarbonate ions

NaHCO₃ had a major effect on MO removal efficiency and reaction rate constant; in other words, with an increase in the NaHCO₃ concentration, pH rose from 6.5 to 9.1, thus increasing MO removal efficiency. Such an increase results from an increase in pH and ionic strength in high NaHCO₃ concentrations [35,36]. The pollutant removal efficiency reached 82.4% at the NaHCO₃ concentration of 800 ppm, which was less than 84.1% for MO removal efficiency without mineral salts concentrations at pH = 9 ($k_{\text{H}_2\text{O}} = 19.31 \text{ day}^{-1}$). This is because the presence of HCO₃⁻ consumes hydroxyl radicals and generates lower reactive of CO₃^{•-} [37], thus declining MO removal efficiency [38].

3.4.3. Sulfate ions

According to Table 6, a rise in the concentrations of Na₂SO₄ and MgSO₄ from 50 to 800 ppm had deactivation effects on the dye removal efficiency and reaction rate constant ($k_{\text{Na}_2\text{SO}_4,800} = 13.01 \text{ day}^{-1}$ and $k_{\text{MgSO}_4,800} = 12.34 \text{ day}^{-1}$) mainly because SO₄^{•-} produced by the reaction of SO₄²⁻ with positive holes and hydroxyl radicals was less reactive [39], which

caused a drop in MO removal efficiency and reaction rate constant.

In a study conducted by Zabat et al. in 2019, the effects of some mineral salts such as NaCl, CaCl₂, and Na₂SO₄ with concentrations of 500 ppm on MO removal efficiency were examined. The results revealed that all inorganic anions had inhibitory effects on MO discoloration efficiency; therefore, an 37.5% decrease in the dye removal efficiency with CaCl₂ was observed [40].

A kinetic study of mineral salts on MO removal efficiency was conducted under optimal conditions (MO concentration = 20 ppm, catalyst dosage = 1 g/L, irradiation time = 120 min, and pH = 6.5). The results of Eq. (5) proved the viability of the first-order kinetic model for MO removal efficiency due to its high determination coefficient values (r^2). The values of k and r^2 are presented in Table 6.

3.5. Recoverability of TiO₂/ZnFe₂O₄/glycine catalyst for MO removal efficiency

Reusability of TiO₂/ZnFe₂O₄/glycine catalyst for the treatment of MO from aqueous solution was investigated under optimal conditions (dye concentration = 20 ppm, catalyst dosage = 1 g/L, irradiation time = 120 min, and pH = 6.5). The results illustrated that the catalyst was still stable after repeating the experiments five times (MO removal efficiency = 80%). As a

result, $\text{TiO}_2/\text{ZnFe}_2\text{O}_4/\text{glycine}$ catalyst gained high stability and recoverability for MO removal efficiency. MO removal efficiency with $\text{TiO}_2/\text{ZnFe}_2\text{O}_4$ catalyst was examined under optimal conditions. The results indicated that there was a 20% increase in MO removal efficiency while coating by glycine.

3.6. Comparison of MO removal efficiency with recent photocatalytic research

Some studies have reported the application of photocatalytic processes to removing MO from contaminated water in recent years. Table 7 presents a comparison of MO removal efficiency achieved in this study with that in other recent studies under optimal conditions. The

results illustrated that $\text{TiO}_2/\text{ZnFe}_2\text{O}_4/\text{glycine}$ catalyst was the most efficient one in removing MO (80%). In addition, to the best of the author's knowledge, only this study investigated the effects of dissolved mineral salts on MO removal efficiency. In this respect, the synthesized $\text{TiO}_2/\text{ZnFe}_2\text{O}_4/\text{glycine}$ catalyst under UV irradiation can be employed as an effective process for treating MO dye from polluted water in the presence of mineral salts, pointing to the novelty of this study.

4. Conclusions

The results indicated that MO concentration, irradiation time, pH, and catalyst dosage had maximum

Table 7. Comparison of MO removal efficiency via photocatalytic processes in recent years.

Catalyst	Operational conditions	MO removal efficiency (%)	Reference
$\text{ZnFe}_2\text{O}_4/\text{SnS}_2$	[Catalyst]: 1 g/L, [MO]: 50 mg/L, Irradiation time: 120 min, pH: 3, H_2O_2 dosage: 2 mL, Xenon lamp	99	[41]
$\text{La}_2\text{NiO}_4/\text{ZnO}$	[Catalyst]: 1g/L, [MO]: 10 mg/L, Irradiation time: 60 min, pH: 7, Solar light	90	[42]
Ag/RP	[Catalyst]: 0.2 g/L, [MO]: 50 mg/L, Irradiation time: 20 min, pH: 7, 300 W Xe lamp	100	[43]
$\text{TiO}_2/\text{ZnO}/\text{rGO}$	[Catalyst]: 0.5 g/L, [MO]: 20 mg/L, Irradiation time: 180 min, pH:7, 6.5 mW/cm ² UV lamp	99.4	[9]
AgBr/g- C_3N_4	[Catalyst]: 0.7 g/L, [MO]: 7 mg/L, Irradiation time: 30 min, pH:6, 100 W Tungsten lamp	69	[44]
$\text{ZnO}/\text{TiO}_2/\text{CdO}$	[Catalyst]: 7 g/L, [MO]: 10 mg/L, Irradiation time: 40 min, pH:7, 200 W Vis-Tungsten-bulb	98	[7]

Table 7. Comparison of MO removal efficiency via photocatalytic processes in recent years (continued).

Catalyst	Operational conditions	MO removal efficiency (%)	Reference
CdS/ZnFe ₂ O ₄	[Catalyst]: 1 g/L, [MO]: 20 mg/L, Irradiation time: 80 min, 500 W Xe long arc lamp	90 >	[15]
Fe _x O _y /TiO ₂ /Au	[Catalyst]: 0.35 g/L, [MO]: 10 mg/L, Irradiation time: 300 min, 150 W Xe lamp	50 >	[45]
Ag doped ZnO nanorods	[Catalyst]: 10 mg, [MO]: 10 mg/L, Irradiation time: 120 min, 10 W UV lamp	88	[3]
TiO ₂ /ZnFe ₂ O ₄ /Glycine	[Catalyst]: 1 g/L, [MO]: 20 mg/L, Irradiation time: 120 min, pH: 6.5, 11 W UV lamp	80	This study

effects on MO removal efficiency. The dye removal efficiency was 80% under the optimal process conditions (MO concentration: 20 ppm, TiO₂/ZnFe₂O₄/glycine catalyst dosage: 1 g/L, irradiation time: 120 min, and pH: 6.5). Low concentrations of NaCl, KCl, and CaCl₂ had adverse effects on MO removal efficiency and reaction rate constant, while ionic strength of NaCl, KCl, and CaCl₂ at their high levels enhanced the dye removal efficiency and reaction rate constant. A rise in the concentrations of Na₂SO₄ and MgSO₄ resulted in deactivation effects on the pollutant removal efficiency and reaction rate constant. Further, the dye removal efficiency and reaction rate constant increased in the presence of NaHCO₃. Based on the findings of this study, the TiO₂/ZnFe₂O₄/glycine/UV light catalyst could be regarded as an efficient process for the treatment of MO from aqueous solution. For future research, it is suggested that simultaneous effects of the mineral salts on the contaminated water and their interactions be studied.

Acknowledgements

The authors appreciate the support of Environmental

Research Institute and Central Laboratory of University of Isfahan.

References

- Das, T.R. and Sharma, P.K. "Bimetal oxide decorated graphene oxide (Gd₂O₃/Bi₂O₃@GO) nanocomposite as an excellent adsorbent in the removal of methyl orange dye", *Materials Science in Semiconductor Processing*, **105**, p. 104721 (2020).
- Fradj, A.B., Boubakri, A., Hafiane, A., and Hamouda, S.B. "Removal of azoic dyes from aqueous solutions by chitosan enhanced ultrafiltration", *Results in Chemistry*, **2**, p. 100017 (2020).
- Bhatti, M.A., Shah, A.A., Almani, K.F., Tahira, A., Chalangar, S.E., dad Chandio, A., Nur, O., Willander, M., and Ibupoto, Z.H. "Efficient photo catalysts based on silver doped ZnO nanorods for the photo degradation of methyl orange", *Ceramics International*, **45**(17), Part B, pp. 23289–23297 (2019).
- Zhu, Z., Xiang, M., Li, P., Shan, L., and Zhang, P. "Surfactant-modified three-dimensional layered double hydroxide for the removal of methyl orange and rhodamine B: Extended investigations in binary dye systems", *Journal of Solid State Chemistry*, **288**, p. 121448 (2020).

- Gautam, P.K., Singh, A., Misra, K., Sahoo, A.K., and Samanta, S.K. "Synthesis and applications of biogenic nanomaterials in drinking and wastewater treatment", *Journal of Environmental Management*, **231**, pp. 734–748 (2019).
- Gautam, P.K., Shivapriya, P.M., Banerjee, S., Sahoo, A.K., and Samanta, S.K. "Biogenic fabrication of iron nanoadsorbents from mixed waste biomass for aqueous phase removal of alizarin red S and tartrazine: Kinetics, isotherm, and thermodynamic investigation", *Environmental Progress and Sustainable Energy*, **39**(2), p. e13326 (2020).
- Upadhyay, G.K., Rajput, J.K., Pathak, T.K., Pal, P.K., and Purohit, L.P. "Tailoring and optimization of hybrid ZnO:TiO₂:CdO nanomaterials for advance oxidation process under visible light", *Applied Surface Science*, **509**, p. 145326 (2020).
- Arshad, R., Bokhari, T.H., Javed, T., Bhatti, I.A., Rasheed, S., Iqbal, M., Nazir, A., Naz, S., Khan, M.I., Khosa, M.K.K., and Zia-ur-Rehman, M. "Degradation product distribution of reactive red-147 dye treated by UV/H₂O₂/TiO₂ advanced oxidation process", *Journal of Materials Research and Technology*, **9**(3), pp. 3168–3178 (2020).
- Nguyen, C.H., Tran, M.L., Van Tran, T.T., and Juang, R.S. "Enhanced removal of various dyes from aqueous solutions by UV and simulated solar photocatalysis over TiO₂/ZnO/rGO composites", *Separation and Purification Technology*, **232**, p. 115962 (2020).
- Dutta, V., Sharma, S., Raizada, P., Hosseini-Bandegharai, A., Kaushal, J., and Singh, P. "Fabrication of visible light active BiFeO₃/CuS/SiO₂ Z-scheme photocatalyst for efficient dye degradation", *Materials Letters*, **270**, p. 127693 (2020).
- Taghvaei, H., Farhadian, M., Davari, N., and Maazi, S. "Preparation, characterization and photocatalytic degradation of methylene blue by Fe³⁺ doped TiO₂ supported on natural zeolite using response surface methodology", *Advances in Environmental Technology*, **3**(4), pp. 205–216 (2017).
- Gautam, P.K., Shivalkar, S., and Samanta, S.K. "Environmentally benign synthesis of nanocatalysts: Recent advancements and applications", *Handbook of Nanomaterials and Nanocomposites for Energy and Environmental Applications*, O.V. Kharissova, L.M.T. MartÍnez and B.I. Kharisov, Eds., pp. 1–19, Cham: Springer International Publishing (2020).
- Davari, N., Farhadian, M., Nazar, A.R.S., and Homayoonfal, M. "Degradation of diphenhydramine by the photocatalysts of ZnO/Fe₂O₃ and TiO₂/Fe₂O₃ based on clinoptilolite: Structural and operational comparison", *Journal of Environmental Chemical Engineering*, **5**(6), pp. 5707–5720 (2017).
- Kaiba, A., Ouerghi, O., Geesi, M.H., Elsanousi, A., Belkacem, A., Dehbi, O., Alharthi, A.I., Alotaibi, M.A., and Riadi, Y. "Characterization and catalytic performance of Ni-Doped TiO₂ as a potential heterogeneous nanocatalyst for the preparation of substituted pyridopyrimidines", *Journal of Molecular Structure*, **1203**, pp. 127376 (2020).
- Zou, L., Wang, H., Jiang, X., Yuan, G., and Wang, X. "Enhanced photocatalytic efficiency in degrading organic dyes by coupling CdS nanowires with ZnFe₂O₄ nanoparticles", *Solar Energy*, **195**, pp. 271–277 (2020).
- Aram, M., Farhadian, M., Nazar, A.R.S., Tangestaninejad, S., Eskandari, P., and Jeon, B.H. "Metronidazole and cephalexin degradation by using of urea/TiO₂/ZnFe₂O₄/clinoptilolite catalyst under visible-light irradiation and ozone injection", *Journal of Molecular Liquids*, **304**, p. 112764 (2020).
- Ai, J., Hu, L., Zhou, Z., Cheng, L., Liu, W., Su, K., Zhang, R., Chen, Z., and Li, W. "Surfactant-free synthesis of a novel octahedral ZnFe₂O₄/graphene composite with high adsorption and good photocatalytic activity for efficient treatment of dye wastewater", *Ceramics International*, **46**(8), Part B, pp. 11786–11798 (2020).
- Choi, I.A., Kwak, D.H., Han, S.B., Park, J.Y., Park, H.S., Ma, K.B., Kim, D.H., Won, J.E., and Park, K.W. "Doped porous carbon nanostructures as non-precious metal catalysts prepared by amino acid glycine for oxygen reduction reaction", *Applied Catalysis B: Environmental*, **211**, pp. 235–244 (2017).
- Mozaffari, M., Arani, M.E., and Amighian, J. "The effect of cation distribution on magnetization of ZnFe₂O₄ nanoparticles", *Journal of Magnetism and Magnetic Materials*, **322**(21), pp. 3240–3244 (2010).
- Zhu, X., Zhang, F., Wang, M., Ding, J., Sun, S., Bao, J., and Gao, C. "Facile synthesis, structure and visible light photocatalytic activity of recyclable ZnFe₂O₄/TiO₂", *Applied Surface Science*, **319**, pp. 83–89 (2014).
- Nguyen, T.B., Huang, C.P., and Doong, R.A. "Photocatalytic degradation of bisphenol A over a ZnFe₂O₄/TiO₂ nanocomposite under visible light", *Science of The Total Environment*, **646**, pp. 745–756 (2019).
- Xu, Q., Feng, J., Li, L., Xiao, Q., and Wang, J. "Hollow ZnFe₂O₄/TiO₂ composites: High-performance and recyclable visible-light photocatalyst", *Journal of Alloys and Compounds*, **641**, pp. 110–118 (2015).
- Meng, X., Zhuang, Y., Tang, H., and Lu, C. "Hierarchical structured ZnFe₂O₄@SiO₂@TiO₂ composite for enhanced visible-light photocatalytic activity", *Journal of Alloys and Compounds*, **761**, pp. 15–23 (2018).
- Zangeneh, H., Zinatizadeh, A.A., Zinadini, S., Feyzi, M., Rafiee, E., and Bahnemann, D.W. "A novel L-Histidine (C, N) codoped-TiO₂-CdS nanocomposite for efficient visible photo-degradation of recalcitrant compounds from wastewater", *Journal of Hazardous Materials*, **369**, pp. 384–397 (2019).

25. Nguyen, T.B. and Doong, R.A. "Fabrication of highly visible-light-responsive $\text{ZnFe}_2\text{O}_4/\text{TiO}_2$ heterostructures for the enhanced photocatalytic degradation of organic dyes", *RSC Advances*, **6**(105), pp. 103428–103437 (2016).
26. Davari, N., Farhadian, M., and Solaimany Nazar, A.R. "Synthesis and characterization of Fe_2O_3 doped ZnO supported on clinoptilolite for photocatalytic degradation of metronidazole", *Environmental Technology*, pp. 1–13 (2019).
27. Khaki, M.R.D., Shafeeyan, M.S., Raman, A.A.A., and Daud, W.M.A.W. "Evaluating the efficiency of nano-sized Cu doped TiO_2/ZnO photocatalyst under visible light irradiation", *Journal of Molecular Liquids*, **258**, pp. 354–365 (2018).
28. Nguyen, C.H., Fu, C.C., and Juang, R.S. "Degradation of methylene blue and methyl orange by palladium-doped TiO_2 photocatalysis for water reuse: Efficiency and degradation pathways", *Journal of Cleaner Production*, **202**, pp. 413–427 (2018).
29. Chen, H., Xue, C., Cui, D., Liu, M., Chen, Y., Li, Y., and Zhang, W. " $\text{Co}_3\text{O}_4\text{-Ag}$ photocatalysts for the efficient degradation of methyl orange", *RSC Advances*, **10**(26), pp. 15245–15251 (2020).
30. Mazhari, M.P., Hamadian, M., Mehpour, M., and Jabbari, V. "Central composite design (CCD) optimized synthesis of $\text{Fe}_3\text{O}_4@\text{SiO}_2@\text{AgCl}/\text{Ag}/\text{Ag}_2\text{S}$ as a novel magnetic nano-photocatalyst for catalytic degradation of organic pollutants", *Journal of Environmental Chemical Engineering*, **6**(6), pp. 7284–7293 (2018).
31. Nguyen, T.D., Phan, N.H., Do, M.H., and Ngo, K.T. "Magnetic Fe_2MO_4 (M:Fe, Mn) activated carbons: Fabrication, characterization and heterogeneous Fenton oxidation of methyl orange", *Journal of Hazardous Materials*, **185**(2), pp. 653–661 (2011).
32. Smith, Y.R., Kar, A., and Subramanian, V. "Investigation of physicochemical parameters that influence photocatalytic degradation of methyl orange over TiO_2 Nanotubes", *Industrial and Engineering Chemistry Research*, **48**(23), pp. 10268–10276 (2009).
33. Rioja, N., Zorita, S., and Penas, F.J. "Effect of water matrix on photocatalytic degradation and general kinetic modeling", *Applied Catalysis B: Environmental*, **180**, pp. 330–335 (2016).
34. Aguedach, A., Brosillon, S., and Morvan, J. "Influence of ionic strength in the adsorption and during photocatalysis of reactive black 5 azo dye on TiO_2 coated on non woven paper with SiO_2 as a binder", *Journal of Hazardous Materials*, **150**(2), pp. 250–256 (2008).
35. Chen, P., Zhang, Q., Shen, L., Li, R., Tan, C., Chen, T., Liu, H., Liu, Y., Cai, Z., Liu, G., and Lv, W. "Insights into the synergetic mechanism of a combined vis-RGO/ TiO_2 /peroxodisulfate system for the degradation of PPCPs: Kinetics, environmental factors and products", *Chemosphere*, **216**, pp. 341–351 (2019).
36. Lair, A., Ferronato, C., Chovelon, J.M., and Herrmann, J.M. "Naphthalene degradation in water by heterogeneous photocatalysis: An investigation of the influence of inorganic anions", *Journal of Photochemistry and Photobiology A: Chemistry*, **193**(2), pp. 193–203 (2008).
37. Farhadian, M., Entezami, N., and Davari, N. "Removal of metronidazole antibiotic pharmaceutical from aqueous solution using $\text{TiO}_2/\text{Fe}_2\text{O}_3/\text{GO}$ photocatalyst: Experimental study on the effects of mineral salts", *Advances in Environmental Technology*, **5**(1), pp. 55–65 (2019).
38. El Hassani, K., Kalnina, D., Turks, M., Beakou, B.H., and Anouar, A. "Enhanced degradation of an azo dye by catalytic ozonation over Ni-containing layered double hydroxide nanocatalyst", *Separation and Purification Technology*, **210**, pp. 764–774 (2019).
39. Dugandžić, A.M., Tomašević, A.V., Radišić, M.M., Šekuljica, N.Ž., Mijin, D.Ž., and Petrović, S.D. "Effect of inorganic ions, photosensitisers and scavengers on the photocatalytic degradation of nicosulfuron", *Journal of Photochemistry and Photobiology A: Chemistry*, **336**, pp. 146–155 (2017).
40. Zabat, N. "Nickel-substituted polyoxometalate nanomaterial as a green and recyclable catalyst for dye decolorization", *Arabian Journal for Science and Engineering*, **44**(1), pp. 227–236 (2019).
41. Zhou, J., Zhang, Z., Kong, X., He, F., Zhao, R., Wu, R., Wei, T., Wang, L., and Feng, J. "A novel P-N heterojunction with staggered energy level based on ZnFe_2O_4 decorating SnS_2 nanosheet for efficient photocatalytic degradation", *Applied Surface Science*, **510**, p. 145442 (2020).
42. Lahmar, H., Benamira, M., Douafer, S., Messaadia, L., Boudjerda, A., and Trari, M. "Photocatalytic degradation of methyl orange on the novel heterosystem $\text{La}_2\text{NiO}_4/\text{ZnO}$ under solar light", *Chemical Physics Letters*, **742**, pp. 137132 (2020).
43. Dou, R., Lin, H., Guo, M., Cao, J., Liu, C., and Chen, S. "Fabrication of Ag/RP composite with excellent photocatalytic activity for degrading high concentration of methyl orange solution", *Materials Letters*, **268**, pp. 127612 (2020).
44. Ghattavi, S. and Nezamzadeh-Ejehieh, A. "A visible light driven $\text{AgBr}/\text{g-C}_3\text{N}_4$ photocatalyst composite in methyl orange photodegradation: Focus on photoluminescence, mole ratio, synthesis method of $\text{g-C}_3\text{N}_4$ and scavengers", *Composites Part B: Engineering*, **183**, pp. 107712 (2020).
45. Boczar, D., Kęcki, T., and Skompska, M. "Visible-light driven $\text{Fe}_x\text{O}_y/\text{TiO}_2/\text{Au}$ photocatalyst-synthesis, characterization and application for methyl orange photodegradation", *Journal of Electroanalytical Chemistry*, **859**, pp. 113829 (2020).

Biographies

Mahboube Hajiali is a PhD student in Chemical Engineering, Faculty of Engineering, University of

Isfahan, Iran. Her main research interests include water and wastewater treatment and environmental engineering in the field of chemical engineering.

Mehrdad Farhadian is currently an Associate Professor in the Chemical Engineering, Faculty of Engineering, University of Isfahan, Iran. He is the Head of Environmental Research Institute at University of Isfahan, Iran. His main research interests include water and wastewater treatment and environmental engineering in the field of chemical engineering.

Shadi Aflaki received her MSc degree in Chemical Engineering, from Faculty of Engineering, University of Isfahan, Iran. Her main research interests include water and wastewater treatment and environmental engineering in the field of chemical engineering.

Nila Davari received her MSc degree in Chemical Engineering, from Faculty of Engineering, University of Isfahan, Iran. Her main research interests include water and wastewater treatment and environmental engineering in the field of chemical engineering.